UV-ozone-treated MoO_3 as the hole-collecting buffer layer for high-efficiency solution-processed SQ:$PC_{71}BM$ photovoltaic devices*

Yang Qian-Qian(杨倩倩)[a)b)], Yang Dao-Bin(杨道宾)[c)], Zhao Su-Ling(赵谡玲)[a)b)†], Huang Yan(黄 艳)[c)‡], Xu Zheng(徐 征)[a)b)], Gong Wei(龚 伟)[a)b)], Fan Xing(樊 星)[a)b)], Liu Zhi-Fang(刘志方)[a)b)], Huang Qing-Yu(黄清雨)[a)b)], and Xu Xu-Rong(徐叙瑢)[a)b)]

[a)] *Key Laboratory of Luminescence and Optical Information (Beijing Jiaotong University), Ministry of Education, Beijing* 100044, *China*
[b)] *Institute of Optoelectronics Technology, Beijing Jiaotong University, Beijing* 100044, *China*
[c)] *College of Chemistry, Sichuan University, Chengdu* 610064, *China*

(Received 24 July 2013; revised manuscript received 1 September 2013; published online 24 January 2014)

The enhanced performance of a squaraine compound, with 2,4-bis[4-(N,N-diisobutylamino)-2,6-dihydroxyphenyl] squaraine as the donor and [6,6]-phenyl-C71-butyric acid methyl ester ($PC_{71}BM$) as the acceptor, in solution-processed organic photovoltaic devices is obtained by using UV-ozone-treated MoO_3 as the hole-collecting buffer layer. The optimized thickness of the MoO_3 layer is 8 nm, at which the device shows the best power conversion efficiency (PCE) among all devices, resulting from a balance of optical absorption and charge transport. After being treated by UV-ozone for 10 min, the transmittance of the MoO_3 film is almost unchanged. Atomic force microscopy results show that the treated surface morphology is improved. A high PCE of 3.99% under AM 1.5 G illumination (100 mW/cm^2) is obtained.

Keywords: organic photovoltaic devices, hole-collecting buffer layer, MoO_3, UV-ozone

PACS: 84.60.Jt, 85.60.Bt, 88.40.hj, 88.40.jr **DOI:** 10.1088/1674-1056/23/3/038405

1. Introduction

There has been tremendous progress in the development of organic photovoltaic devices (OPVs) during the past two decades. Improvements in new materials, device design, and morphological control have led to the power conversion efficiency (PCE) of OPVs moving forward rapidly to 10%.[1–3] However, for large-scale commercialization, the PCE still needs to be improved. So far, both solution processes and thermal evaporation have been used to fabricate OPVs. The solution process has been more widely used due to its easy operation and the potentially low fabrication costs.[4,5] To obtain improved performance, efforts have focused on the design and synthesis of soluble donors with high charge-carrier mobility and absorption in the visible and new-infrared spectral regions, in combination with high interfacial gap energy at the donor–acceptor interface. Polymers used as donors to fabricate solar cells still suffer from some shortcomings, such as batch-to-batch variation, indefinite molecular weight, polydispersity, and impurity. In contrast, small-molecule materials do not intrinsically have such drawbacks. Furthermore, small-molecule organic materials could exhibit higher charge carrier mobility, as well as tuning their band structure more easily to absorb sunlight efficiently.[6] Among the small-molecule materials, owing to their high absorption coefficients and intense absorption in the red and near-infrared (NIR) spectral regions, 2,4-bis[4-(N,N-diisobutylamino)-2,6-dihydroxyphenyl] squaraine (SQ) dyes have shown tremendous potential for OPVs.[7–9] In particular, SQ has a lower highest occupied molecular orbit (HOMO) energy level than that of other commonly used donors such as copper phthalocyanine.[10,11]

Bulk-heterojunction (BHJ) OPVs based on an active layer sandwiched between a transparent conductive anode (e.g., indium tin oxide, ITO) and a low-work-function cathode (e.g., Al, Ca) is the simplest structure. However, in this case, both the donor and acceptor materials in the active layer contact directly with the anode and cathode electrodes, which will result in current leakage due to the transfer of electrons (holes) to the hole-collecting anode (the electron-collecting cathode).[12,13] To solve this problem, an electron blocking and hole collecting buffer layer (HCBL) is usually introduced between the active layer and the transparent anode.[14] Poly(3,4-ethylenedioxythiophene):poly(styrenesulfonate) (PEDOT:PSS) is a commonly employed HCBL in OPVs used to facilitate hole extraction thanks to its high transparency, good conductivity, smooth morphology, and high work function.[15] In addition, PEDOT:PSS as HCBL treated by UV-ozone can improve the performance of OPVs.[16–18] However, it has also been found that PEDOT:PSS is usually acidic and hygroscopic. The high acidity of PEDOT:PSS has been assumed to corrode the ITO electrode, meanwhile, its hygroscopic nature can accelerate cathode oxidation by promoting the infiltration of humidity from the device edges and

*Project supported by the Program for New Century Excellent Talents in University of Ministry of Education of China (Grant No. NCET-10-0220), the Specialized Research Fund for the Doctoral Program of Higher Education of China (Grant No. 20120009130005), and the Fundamental Research Funds for the Central Universities of Ministry of Education of China (Grant No. 2012JBZ001).

†Corresponding author. E-mail: slzhao@bjtu.edu.cn
‡Corresponding author. E-mail: huangyan@scu.edu.cn

© 2014 Chinese Physical Society and IOP Publishing Ltd

results in rapid device degradation.[19,20] In our previous study, we found that SQ was sensitive to acidic conditions, and the acidic nature of PEDOT:PSS deteriorated the performance of OPVs based on SQ:$PC_{71}BM$. Because of these drawbacks, several inorganic materials have been proposed to replace PEDOT:PSS as the HCBL, such as NiO,[12] MoO_3,[21–23] WO_3,[24] and V_2O_5.[21] The effects and mechanism of MoO_3 as HCBL in SQ-based solar cells were investigated in another paper. It was concluded that the MoO_3 layer acts as an effective exciton-blocking layer and improves the energy alignment between the anode and the active layer. However, there are still some questions that need to be answered, for example regarding the optimized thickness and the influence of the morphology of MoO_3. Although some surface treatments of MoO_3 have been investigated in polymeric BHJ OPVs,[25] it is necessary to deeply understand the mechanism of UV-ozone-treated MoO_3 on the performance of small-molecule OPVs. In this paper, we explore the enhanced performance of solution-processed SQ:$PC_{71}BM$-based small-molecule organic solar cells via UV-ozone-treated MoO_3 as the hole-collecting buffer layer. The dependence of the thickness of the MoO_3 layer and the time of the UV-ozone treated MoO_3 on photovoltaic device performance was studied.

2. Experiment

Patterned indium tin oxide (ITO)-coated glass substrates with a sheet resistance of 15 Ω/square were cleaned consecutively in an ultrasonic bath containing detergent, acetone, ethanol, and deionized water for 10 min each, and then blow-dried using high-purity nitrogen. The substrates were treated by UV-ozone for 5 min, and then the HCBL was fabricated. MoO_3 films with different thicknesses were thermally evaporated onto ITO substrates under a vacuum of less than 3×10^{-4} Pa at a rate of 0.5 Å/s (1 Å = 0.1 nm). The ITO/MoO_3 samples were then treated by UV-ozone for various times. Subsequently, the photoactive layer was fabricated by spin-coating a blend of the SQ and $PC_{71}BM$ in chloroform with a total concentration of 20 mg/ml under an N_2-filling glove box at 25 °C. The film thickness was measured by surface profilometry. The solution mixture was stirred for 12 h at room temperature, and then the substrates were loaded into a vacuum chamber to deposit LiF (8 Å) and Al (1000 Å) under a pressure of less than 3×10^{-4} Pa at rates of 0.2 Å/s and 1.5 Å/s, respectively. The deposition rate and film thickness were monitored *in situ* using a quartz crystal oscillator mounted onto the substrate holder. The active area was 6×10^{-6} m^2. The current–voltage curves in dark and under illumination were measured using an Abet solar simulator with a Keithley 4200 source measurement unit under AM 1.5 G illumination (100 mW/cm^2), after spectral mismatch correction under an ambient atmosphere at 25 °C. The morphology of the as-grown HCBL thin film was characterized by atomic force microscopy (AFM) in tapping mode. The transmittance spectra were measured by a Shimadzu UV-3101 PC spectrometer under an ambient atmosphere at 25 °C. The energy level diagrams of the different materials used in the device fabrication are shown in Fig. 1.

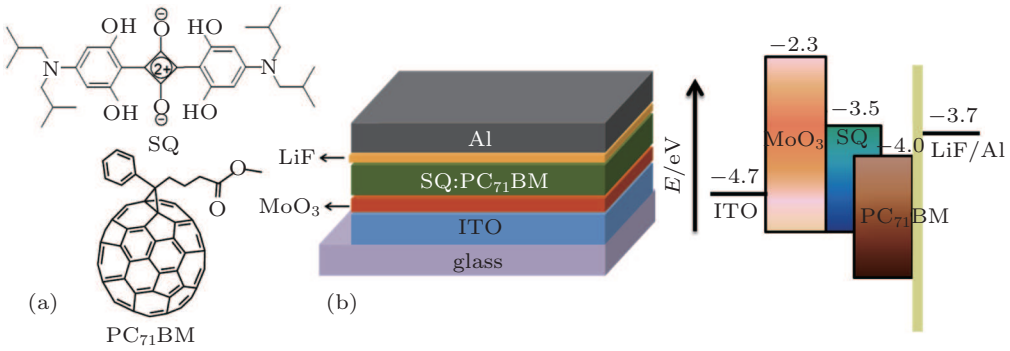


Fig. 1. (color online) (a) The chemical structure of SQ and $PC_{71}BM$. (b) The device structure of the OPVs. (c) The energy level diagram of the OPVs.

3. Results and discussion

First, we investigated the effects of the active layer thickness on the performance of the OPVs. The thickness of the active layer was controlled by changing the spin speeds. OPVs were fabricated with the following structures: ITO/SQ:$PC_{71}BM$/LiF/Al. The current density–voltage (J–V) characteristics for the OPVs with different spin-coated speeds are shown in Fig. 2, and the extracted device parameters are summarized in Table 1. As illustrated in Fig. 2, the open-circuit voltage (V_{OC}) remained almost unchanged at approximately 0.9 V, whereas the short-circuit current density (J_{SC}) was firstly increased and then decreased when the spin-coated speeds were higher than 1500 rad/min. As a consequence, the optimized device exhibits the best PCE of 2.84% with the spin-coated speed at 1500 rad/min.

We believe that V_{OC} is determined by the energy difference between the highest occupied molecular orbital of the donor SQ and the lowest unoccupied molecular orbital of the acceptor $PC_{71}BM$. These two materials are not changed, so V_{OC} remains almost the same. On the other hand, J_{SC} depends

on the mutual influence of light absorption and carrier transport, while a contradicting effect from these two aspects is caused by varying the thickness of the active layer. The thicker the active layer, the more the excitons are induced by light absorption. However, the built-in electric field becomes weaker and the pathway for transporting the opposite charge carriers derived from the exciton separation to their corresponding electrodes becomes longer when the active layer is thick. This means that there is a lower probability of charge collection by the respective electrodes. The highest $J_{SC} = 8.76$ mA/cm^2 is attributed to the balancing between the light absorption and the carrier transport.

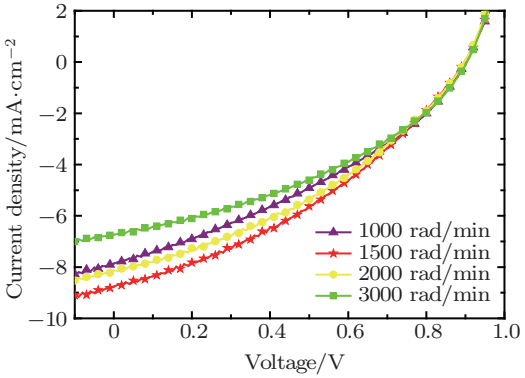


Fig. 2. (color online) The J–V characteristics of OPVs with different spin-coated speeds (1000–3000 rad/min).

Table 1. Photovoltaic performance parameters for devices with different spin-coated speeds (1000–3000 rad/min).

Spin speed/(rad/min)	Thickness/nm	V_{OC}/V	J_{SC}/(mA/cm^2)	FF	PCE/%
1000	112±2	0.90	7.87	0.35	2.48
1500	78±2	0.90	8.76	0.36	2.84
2000	55±2	0.90	8.13	0.37	2.71
3000	42±2	0.90	6.73	0.39	2.36

Next, MoO_3 is employed as the HCBL in OPVs to facilitate the hole extraction because of its high transparency, good conductivity, and easy fabrication (low evaporation temperature, melting point ≈ 795 °C).[23] A sufficient oxide layer thickness is required to form a uniform contact with the active layer to reduce leakage current. Therefore, it is necessary to optimize the MoO_3 layer thickness in order to obtain an optimum device performance. ITO/MoO_3/SQ:PC_{71}BM/LiF/Al OPVs were prepared with different MoO_3 layer thicknesses of 0 nm, 1 nm, 4 nm, 8 nm, and 12 nm respectively. The J–V characteristics of these OPVs are shown in Fig. 3. The dependence of the photovoltaic parameters on MoO_3 thickness is summarized in Table 2. As shown in Fig. 3 and Table 2, the OPVs exhibit obvious performance differences with the change in MoO_3 buffer layer thickness. Firstly, with the insertion of a 1 nm MoO_3 layer, the OPV shows poor performance. This is because that MoO_3 layer is not thick enough to form a continuous film. The ITO substrate is partially covered, with the oxide forming small islands. As a result, the contact between the anode and the active layer has two different interfaces: the ITO/active layer and ITO/MoO_3/active layer. The J–V curve of the device with a 1 nm MoO_3 layer can be thought of as two separate competing curves overlapping each other. Each one that has a different characteristic to the other will bring on the visible concave feature in the resultant J–V curve, as shown in Fig. 3 and results in a poor fill factor (FF) = 0.33. The FF of the device with 4 nm MoO_3 increases to 0.42, and this strongly indicates that these oxide islands are formed continuously on the top of the ITO. With the insertion of a suitably thick MoO_3 layer (8 nm), the performance of the OPVs is remarkably improved. This could be explained by three aspects: (i) the energy alignment between the work function of MoO_3 and the HOMO energy of SQ, which results in holes easily extracted by the anode; (ii) the energy band gap of MoO_3 is around 3 eV, which make MoO_3 act as an effective exciton-blocking layer to mainly prevent electrons from reaching the anode due to the large energy band gap of MoO_3; and (iii) the V_{OC} of the device increases from 0.9 V to 0.95 V after modification. The higher V_{OC} can be expected according to the Shockley equation as a consequence of reduced leakage current (see the inset of Fig. 3). As shown in Table 2, J_{SC}, FF, and PCE increase initially and then drop slightly with the increased thickness of the MoO_3 layer. We conclude that if the thickness of the MoO_3 layer is less than 8 nm, then there is hole transport from the MoO_3 layer to the anode. Meanwhile, the electrons can probably tunnel through the MoO_3 layer and result in the decreased photocurrent. On the other hand, if the thickness of the MoO_3 layer is above 8 nm, then hole transport from the active layer to the anode becomes difficult, and the transmittance of the film will become poor, which also leads to the decreased photocurrent. As a consequence, the optimized device exhibits the best PCE of 3.59% with the MoO_3 layer of 8 nm thanks to the balance between the optical transmission and the charge transport.

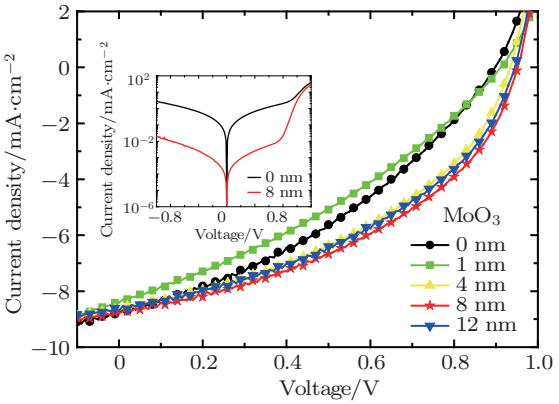


Fig. 3. (color online) The J–V characteristics of OPVs with MoO_3 as the anode modification hole-collecting buffer layer (thicknesses=0 nm, 1 nm, 4nm, 8 nm, and 12 nm). The inset shows the semi-logarithmic current density vs. voltage characteristics of OPVs with 0 nm and 8 nm MoO_3 as the hole-collecting buffer layer in the dark.

Table 2. The photovoltaic performance parameters for devices with MoO_3 as the hole-collecting buffer layer (thicknesses=0 nm, 1 nm, 4 nm, 8 nm, and 12 nm).

MoO_3 thickness/nm	V_{OC}/V	J_{SC}/(mA/cm^2)	FF	PCE/%
0	0.90	8.76	0.36	2.84
1	0.91	8.40	0.33	2.52
4	0.93	8.60	0.42	3.36
8	0.95	8.79	0.43	3.59
12	0.94	8.70	0.42	3.43

UV-ozone surface treatment is widely used to clean and modify the molecular surface of solids. It is capable of cleaning the surface of contaminations, controlling the work function and resistivity of the films, and improving the wettability of the sample surface. OPVs with MoO_3 as the HCBL treated by UV-ozone for different times were fabricated to compare their performance. All the *J*–*V* characteristics are shown in Fig. 4, and the dependence of the photovoltaic parameters on the MoO_3 treatment time is plotted in Fig. 5. As shown in Figs. 4 and 5, the device performance enhancement reaches a peak when the duration of the UV-ozone treatment is increased to 10 min. The highest PCE for UV-ozone-treated MoO_3 devices is 3.99% with J_{SC}, V_{OC}, and FF being 9.23 mA/cm^2, 0.94 V, and 46%, respectively. The PCE slightly decreases when the treatment duration is further increased. In the previous report, during the process of UV-ozone treatment on MoO_3, O_3 can oxidize the small amounts of Mo^{5+} to the Mo^{6+} oxidation state. Therefore, it can enhance the quality of the MoO_3 film in extracting the holes to the anode well.[26] It is necessary to deeply understand the mechanism of UV-ozone-treated MoO_3 on the performance of OPVs.

The inset of Fig. 4 shows the transmittance spectrum of 8 nm thick MoO_3 before and after UV-ozone treatment. It can be seen that the optical transmission across the entire visible spectrum is almost unchanged. This suggests that the transmittance has no evident effect on the improved performance.

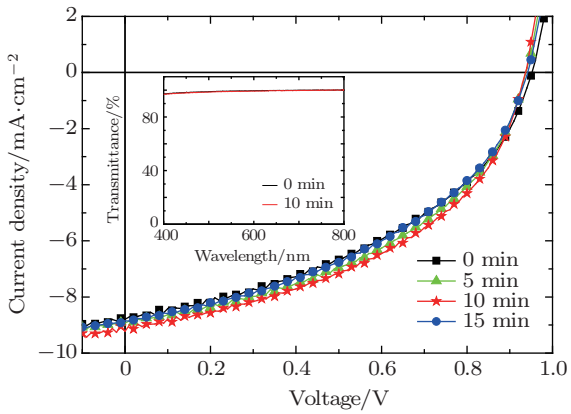


Fig. 4. (color online) The *J*–*V* characteristics of OPVs with UV-ozone-treated MoO_3 as the hole-collecting buffer layer (time = 0 min, 5 min, 10 min, and 15 min). The inset shows the transmittance spectrum of the MoO_3 film before and after UV-ozone treatment.

The external quantum efficiency (EQE) of devices with MoO_3 as the HCBL before and after 10 min of UV-ozone treatment is shown in Fig. 6. For the entire wavelength range, the device with UV-ozone-treated MoO_3 exhibits a higher EQE than the non-UV-ozone-treated one. In addition, there is no noticeable difference in the shape of the EQE spectra among these devices. This provides proof that the active layer in each OPV is similar and has no obvious influence on the EQE. Therefore, performance enhancement with UV-ozone treatment cannot be attributed to the photoactive layer.

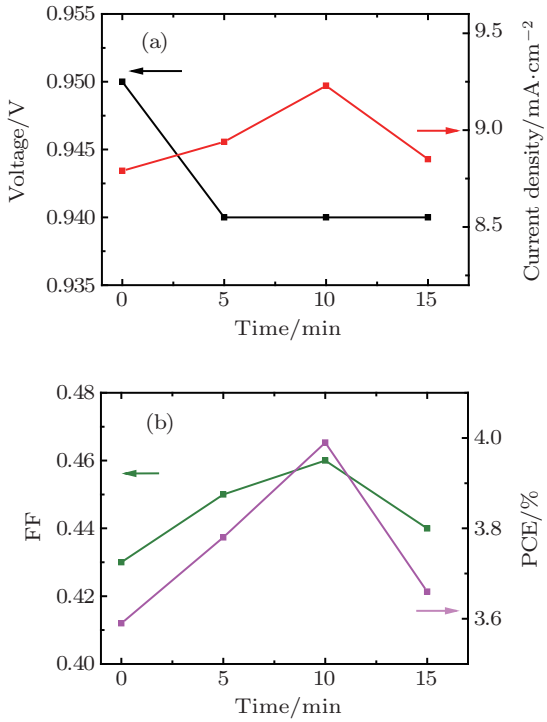


Fig. 5. (color online) The dependence of each parameter on the UV-ozone treatment times in the OPVs (a) V_{OC} and J_{SC}; (b) FF and PCE.

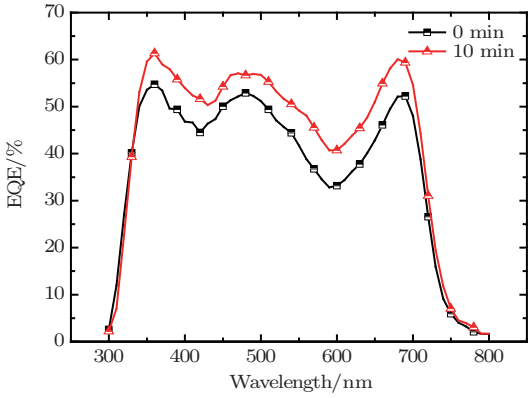


Fig. 6. (color online) EQE as a function of wavelength for devices before and after UV-ozone-treated MoO_3 as the hole-collecting buffer layer.

In order to investigate the origin of the enhancements of J_{SC} and PCE with the surface treatment, we analyzed the surface of the ITO/MoO_3 films. Figure 7 shows the tapping mode AFM images of the ITO/MoO_3 samples treated by UV-ozone for 10 min, and the non-UV-ozone treated for comparison. According to the images, the ITO/MoO_3 film surface is smoothed by the treatment, which may be ascribed to the removal of the contamination. The roughness obtained from the AFM images (Fig. 7(a)) of the non-treated film is 1.83 nm root-mean-square

(rms). In contrast, the roughness of the treated one decreases to 1.67 nm rms (Fig. 7(b)). This more directly indicates that UV-ozone treatment is helpful in smoothing and cleaning the surface. It can be observed that the performance of the device degraded slightly when being treated for longer than 10 min. We believe that the chemisorbed oxygen reaches the maximum and then saturates with the extension of the treatment time. However, a long treatment time may cause unexpected contaminations on the device surface, such as C, S, and -OH, which may degrade the interface properties. Therefore, an appropriate treatment time of 10 min is taken. This relatively good surface roughness of ITO/MoO_3 treated for 10 min favors device fabrication, and the J_{SC} would be improved due to the good interface contact.

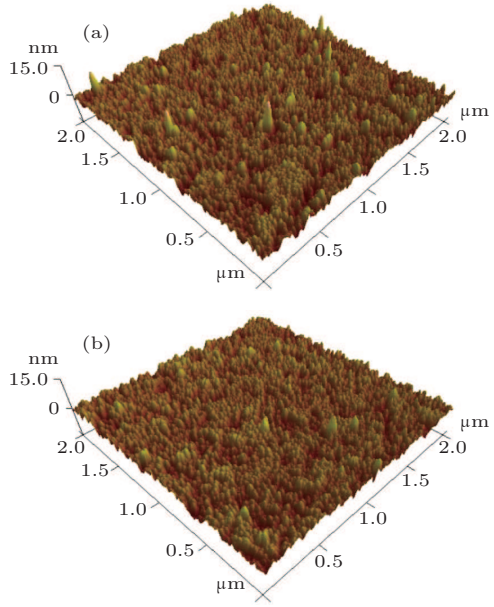


Fig. 7. (color online) AFM showing the morphology of ITO/MoO_3 films (size 2 μm×2 μm) for (a) non-UV-ozone treated, and (b) 10 min UV-ozone treated.

The series resistance (R_S) is derived from the slope of the illuminated J–V curve in the first quadrant. R_S depends on the resistance of the semiconductor bulk, the metal electrodes, and the metal/semiconductor interfaces. The series resistance decreases from an initial value of 11.32 Ω·cm^2 to 8.21 Ω·cm^2 after being treated by UV-ozone for 10 min. Therefore, the smaller value of R_S is beneficial to the performance of the OPVs. From the above, the resistance of the semiconductor bulk and the metal electrodes are almost unchanged after treatment, so the J_{SC} would be improved due to the lower resistance on the metal/semiconductor interfaces.

4. Conclusion

In summary, efficient solution-processed SQ:$PC_{71}BM$ photovoltaic devices using MoO_3 as the hole-collecting buffer layer were fabricated. Although some surface treatments of MoO_3 have been investigated in polymeric BHJ OPVs, we chose a different research subject: a small-molecule material SQ as an active layer. With the insertion of the MoO_3 layer, the performance of the OPVs is remarkably improved. The MoO_3 layer acts as an effective exciton-blocking layer and improves the energy alignment between the anode and the active layer. The optimized device with an 8 nm MoO_3 layer exhibited the best PCE, resulting from a balance of optical absorption and charge transport. After UV-ozone treatment, the surface morphology of the MoO_3 film can be improved, and the J_{SC} will be improved due to the lower resistance on the metal/semiconductor interfaces. This is favorable to the performance of the OPVs. The thickness of the MoO_3 and the UV-ozone treatment time on MoO_3 were 8 nm and 10 min, respectively, resulting in a PCE of 3.99%.

References

[1] He Z C, Zhong C M, Huang X, Wong W Y, Wu H B, Chen L W, Su S J and Cao Y 2011 *Adv. Mater.* **23** 4636
[2] Dou L T, You J B, Yang J, Chen C C, He Y J, Murase S, Moriarty T, Emery K, Li G and Yang Y 2012 *Nat. Photon.* **6** 180
[3] He Z C, Zhong C M, Su S J, Xu M, Wu H B and Cao Y 2012 *Nat. Photon.* **6** 591
[4] Park S H, Roy A, Beaupré S, Cho S, Coates N, Moon J S, Moses D, Leclerc M, Lee K and Heeger A J 2009 *Nat. Photon.* **3** 297
[5] Moulé A J and Meerholz K 2009 *Adv. Funct. Mater.* **19** 3028
[6] Walker B, Tamayo A B, Dang X D, Zalar P, Seo J H, Garcia A, Tantiwiwat M and Nguyen T Q 2009 *Adv. Funct. Mater.* **19** 3063
[7] Wei G D, Wang S Y, Renshaw K, Thompson M E and Forrest S R 2010 *ACS Nano* **4** 1927
[8] Silvestri F, Irwin M D, Beverina L, Facchetti A, Pagani G A and Marks T J 2008 *J. Am. Chem. Soc.* **130** 17640
[9] Chen G, Sasabe H, Wang Z Q, Wang X F, Hong Z, Kido J and Yang Y 2012 *Phys. Chem. Chem. Phys.* **14** 14661
[10] Xue J G, Rand B P, Uchida S and Forrest S R 2005 *J. Appl. Phys.* **98** 124903
[11] Wang N N, Yu J S, Zang Y and Jiang Y D 2010 *Chin. Phys. B* **19** 038602
[12] Irwin M D, Buchholz D B, Hains A W, Chang R P H and Marks T J 2008 *Proc. Natl. Acad. Sci. USA* **105** 2783
[13] Liu X D, Zhao S L, Xu Z, Zhang F J, Zhang T H, Gong W, Yan G, Kong C, Wang Y S and Xu X R 2011 *Chin. Phys. B* **20** 068801
[14] Yang Q Q, Zhao S L, Xu Z, Zhang F J, Yan G, Kong C, Fan X, Zhang Y F and Xu X R 2012 *Chin. Phys. B* **21** 128402
[15] Kirchmeyer S and Reuter K 2005 *J. Mater. Chem.* **15** 2077
[16] Benor A, Takizawa S Y, Bolívar C P and Anzenbacher P 2010 *Org. Electron.* **11** 938
[17] Helander M G, Wang Z B, Greiner M T, Liu Z W, Lian K and Lu Z H 2009 *Appl. Phys. Lett.* **95** 173302
[18] Nagata T, Oh S, Chikyow T and Wakayama Y 2011 *Org. Electron.* **12** 279
[19] Jong M P, IJzendoorn L J and Voigt M J A 2000 *Appl. Phys. Lett.* **77** 2255
[20] Nguyen T P and de Vos S A 2004 *Appl. Surf. Sci.* **221** 330
[21] Shrotriya V, Li G, Yao Y, Chu C W and Yang Y 2006 *Appl. Phys. Lett.* **88** 073508
[22] Li N, Lassiter B E, Lunt R R, Wei G D and Forrest S R 2009 *Appl. Phys. Lett.* **94** 023307
[23] Sun Y M, Takacs C J, Cowan S R, Seo J H, Gong X, Roy A and Heeger A J 2011 *Adv. Mater.* **23** 2226
[24] Long Y B 2010 *Sol. Energy Mater. Sol. Cells* **94** 744
[25] Cheng F, Fang G J, Fan X, Huang H H, Zheng Q, Qin P L, Lei H W and Li Y F 2013 *Sol. Energy Mater. Sol. Cells* **110** 63
[26] Deng Z B, Lü Z Y, Xu D H, Xiao J and Wang Y S 2012 *Solid-State Electron.* **76** 25